University of Reading

Capillary transport in particulate porous materials at low levels of saturation: the mathematical model and a comparison with experimental observations

by

Vladimir Mitkin, Theo G. Theofanous and

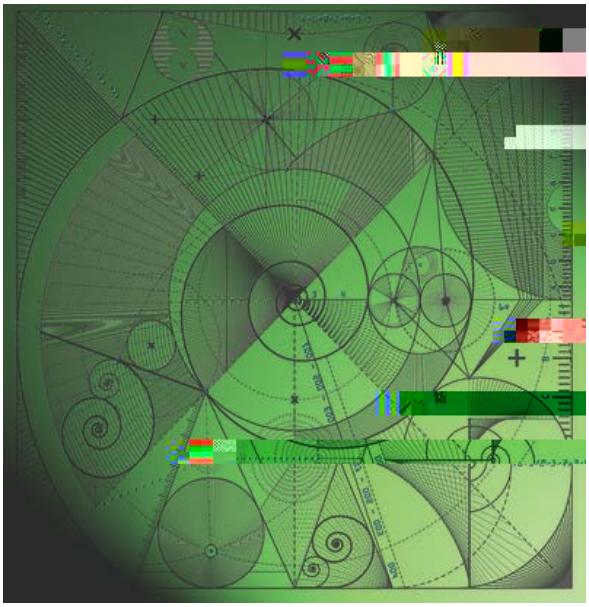

Capillary transport in particulate porous materials at low levels of saturation: the mathematical model and a comparison with experimental observations.

Alex V. Lukyanov [y], Vladimir Mitkin [z], Theo G. Theofanous [x] and Mike Baines [y]
[y] School of Mathematical and Physical Sciences, University of Reading, Reading, RG6 6AX, UK
[z] Aerospace Research Laboratory, University of Virginia, Charlottesville, VA 22903, USA and
[x] University of California, Santa Barbara, CA 93106, USA

We have established previously, in a pilot study, that the spreading of liquids in granular porous materials at low levels of saturation, typically less than 10% of the available void space, has very distinctive features in comparison to that at higher saturation levels. In particular, it has been shown, on theoretical grounds, that the spreading is controlled by a special type of di usional process, that its physics can be captured by an equation of the super-fast di usion class, and that these ndings were supported by rst-of-a-kind experiments. In this paper, we take these ndings to the next level including deeper examination and exposition of the theory, an expanded set of experiments to address scaling properties, and systematic evaluations of the predictive performance against these experimental data, keeping in mind also potential practical applications.

I. INTRODUCTION

Even a small amount of a liquid added to a dry granular material may dramatically change its structural properties due to the appearance of a strong capillary cohesion force between the particles [1{4]. The strong capillary force, of the order of F 2 R cos $_c$, is due to the liquid bridges (pendular rings) formed at the point of particle contact [5, 6]. Here, R is the average particle radius, is the surface tension coe cient and $_c$ is the static contact angle of the liquid formed at the three-phase contact line on the at surface of the solid. A simple estimate for water at room temperature (= 72 mN=m) and sand particles ($_c$ = 30) of 400 m in diameter results in F 8 10 ^{5} N, which is much larger than the gravity force acting on each particle 8 10 ^{8} N. It is interesting to note, that the cohesive force is practically independent of the liquid content, that is the value of saturation, as25(ec$_R$h(as)t(he)-325(t)]TJ count,326(ha6 Tf le8(t,3d)-sist)-326(a7 T6(alue)]TJ 0 -11.45isolatede8(33(25(indep)ul25(e
can be interpreted as the characteristic average thickness of the surface roughness. For example, a threshold value s_0 0:2% has been observed in experiments using spherical particles, average radius R = 187:5 m, with the maximum surface roughness amplitude of approximately 500 nm as determined by scanning force microscopy [1]. At the same time, in our experiments with Ottawa sands, average grain radius R 250 m with the surface roughness amplitude distributed between 250 nm and 3 m [9], a minimal value of s_0 0:6% was observed, implying an e ective $_R$ value of 1:5 m. One can see that the lower is the surface roughness on average, the lower is the critical value s_0.

If we now consider spherical (or nearly spherical) grains and take into account that only some part of the volume 4 R ^{2} $_R$ is available for the liquid during the spreading, then the value of saturation due to the liquid distributed

on the rough surface of the grains is

$$s_0 = 3 \; {}_R \frac{1}{\frac{R}{R}}; \qquad (1)$$

where parameter

Set	Liquid

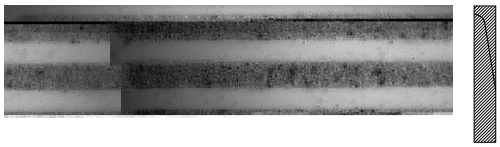

FIG. 6. Channels in Te on (diameter of the hemicylinder d_c = 6:15 mm) lled in by the standard Ottawa sand (R 0:25 mm) before depositing V_D = 3 mm^3 liquid drops.

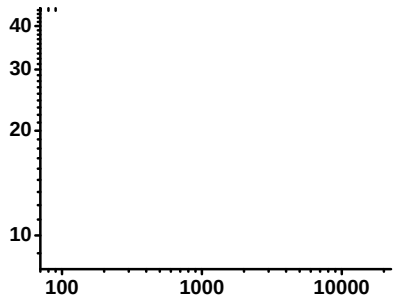

FIG. 7. Spreading of TCP, TEHP and TBP liquid drops (V_D = 3 mm^3) in R 0:25 mm sand in the channels, as in Fig. 6. Normalised wet volume V =V_D (inverse average saturation s ^{1}) as a function of time. The experimental data are shown by symbols and the solid lines (brown) are the ts V =V_D = A + Bt$^{0:5}$.

Using (3) and (4), the average capillary bridge pressure P = < p > ^{l} can be presented as

$$P = p_0 \frac{C_1 A_s^{1=2}}{(s \quad s_0)^{1=2}}; \qquad (5)$$

where < ::: > ^{l} = V_l ^{1} $\int_{V_l}$ d^{3}x is intrinsic liquid averaging, V_l is liquid volume within the sample volume V . We have assumed previously in developing our preliminary theoretical model that parameter s_0 is constant, that is independent of the capillary pressure. This is a good approximation in a range of capillary pressures, but could be possibly violated at small values of s s_f s_0. Indeed, consider a model groove geometry shown in Fig. 8. Surface ows in that kind of geometry have been studied experimentally and theoretically in [10{12]. The liquid in this case is contained both inside the large scale grooves (large scale surface roughness), in capillary menisci, and on the surface with much smaller scale roughness. At very large capillary pressure, the meniscus curvature could be much

mensions [19, 20], obeys a Darcy-like law

$$q = \frac{m}{} r \quad ; \qquad (7)$$

where is liquid viscosity, is local pressure in the liquid averaged within the surface roughness and $_m = _0 \frac{2}{R}$ is the e ective coe cient of permeability of the surface roughness, which is proportional to the square of the length scale parameter $_R$. To understand the order of magnitude of $_m = _0 \frac{2}{R}$, one can again consider the surface groove of a simpli ed geometry, as is shown in Fig. 8. We note, that the uid ow mostly occurs within large scale surface grooves. Then, assuming a fully developed rectilinear Hagen-Poiseuille ow in the open channel at $_0 = = 2$ and $_c = 0$, Fig. 8, and the results of analysis of liquid ows in corners in [21], $_0 = \frac{"_0}{_1} 1 \frac{}{4}$, where non-dimensional parameter $_1$ was found to be $_1 \quad 100$ [21] and parameter $"_0 < 1$ is the ratio of the total cross sectional area of the grooves to the total cross sectional area of the surface layer of width $_R$. Due to the capillary pressure variations in the grooves and, as a consequence, variations of the cross-section area of the groove volume occupied by the liquid, parameter $_0$ would vary in the idealized case between $\frac{"_0}{_1} 1 \frac{}{4} \quad _0 \quad \frac{"_0}{_2}$, where parameter $_2$ in the case of a fully saturated groove was found to be $_2 \quad 50$ [21]. This implies that $_0 = _0(s)$. When s changes from s_f to s_c, assuming again a linear relationship

$$_0(s) = \frac{\frac{2}{0} \quad \frac{1}{0}}{s_c \quad s_f}(s \quad s_f) + \frac{1}{0};$$

$$\frac{1}{0} = \frac{"_0}{_1} 1 \frac{}{4} \quad ; \qquad \frac{2}{0} = \frac{"_0}{_2}:$$

The minimum value of the channel permeability is de- ned by the maximum capillary pressure in the system. We note, while in unbounded V-shaped grooves, especially at small opening angles $_0$, the free surface is also unbounded, so that the capillary spreading in the absence of external forces, like the gravity force, is unbounded, in our case, a quasi-steady state is observed corresponding to the maximum capillary pressure [22]. If the contact angle $_c$ is not equal to zero, then the amount of the liquid contained in the groove at a xed value of pressure, that is at a xed value of $_R$ is reduced. Then

$$\frac{1}{0} = \frac{"_0}{_1} \cos _c(\cos _c \quad \sin _c) \quad \overline{5.39\ 014}$$

To obtain analytical results, we restrict ourselves to the case of a spherical particle of radius R. In this case, domain boundaries $@_1$ and $@_2$ will be circular cross

and

$$vj_{@} = \frac{1}{s_f} \frac{u_0^{\frac{3}{2}}}{\ln u_0} \frac{@u}{@x_{@}} \quad ; \qquad (24)$$

where $u = s \quad s_f$ and u_0

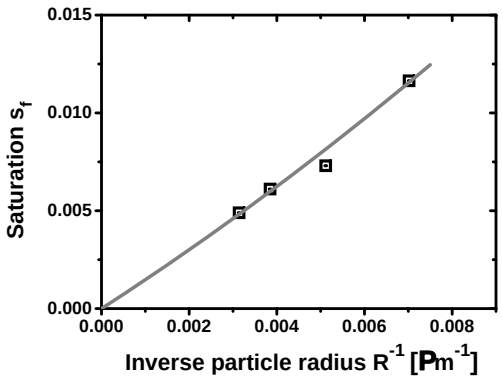

FIG. 10. Saturation s_f as a function of R^{-1} shown by symbols. The solid line is the fit $s_f = A_f R^{-1} + B_f R^{-2}$ at $A_f = 1.5$ μm and $B_f = 29$ μm^2.

can present (22) in non-dimensional form by normalizing distances $\tilde{x} = x/L_0$ and time $\tilde{t} = t/t_0$. As the characteristic length scale, we use the wet spot radius L_0 at some moment of time, which will be initial time for simulations $\tilde{t} = 0$, and $t_0 = L_0^2/D_0^e$. Then, omitting tilde in the notations, equation (22) can be presented as

$$\frac{\partial s}{\partial t} = \frac{c_0(s)\,(1-s)}{|\ln(1-s_0^e)|\,(1-s_0^e)^{3/2}}; \qquad (26)$$

with two boundary conditions

$$s|_{x=1} = s_f \qquad (27)$$

and

$$v_n|_{x=1} = \frac{c_0(s)\,(n\cdot r)\,s}{s_f\,|\ln(1-s_f)|\,(1-s_f)^{3/2}}. \qquad (28)$$

Here

$$D_0^e = \frac{3}{R^2}\int_0^{R} P_c\,dr \qquad (29)$$

and

$$c_0(s) = \frac{2/3 - 1/3}{s_c - s_0^e}(s - s_0^e) + 1$$

in

$$s_0^e \le s \le s_c$$

otherwise

$$c_0(s) = 2/3 - 1/3.$$

So, the problem has three essential non-dimensional parameters s_f; $s_f - s_0^e$ and $V_D = L_0^3$. The last parameter only contributes through the initial profile of saturation $s(x,0)$ at $t = 0$. We have already seen that variations of initial drop volume V_D at $s_f = \text{const}$ and $s_f - s_0^e = \text{const}$ result in self-similar behaviour, such that evolution curves of the moving front collapse on a single master curve after re-normalizing time t by a factor of $V_D^{2/3}$. This implies that one can further assume that L_0^3 / V_D, so that parameter L_0 can be solely defined by the initial drop volume V_D. This leaves us with just two non-dimensional

$$\frac{@s}{@t} = r \quad \frac{c_0(s)\, g(s)\, r\ s}{j \ln(s \quad s_0^e) j (s \quad s_0^e)^{3=2}} \quad ; \qquad (30)$$

where augmenting permeability function g(s), Fig. 11,

$$g(s) = 1 + f_0\, 10^{\ {}_g s \quad {}_g} \qquad (31)$$

with

$${}_g = 16{:}5; \quad {}_g = 1{:}65$$

and

$$f_0 = \left(\frac{R}{R_m} \right)^{2} - \frac{{}_w}{{}_w}: \qquad (32)$$

The values of the coe cients in (31) have been chosen such that, according to [31], in the medium ne sands (R_m 260 m) and water (surface tension ${}_w$ and viscosity ${}_w$)

$$g(s)\, j_{s=0\ :1} = 2; \quad g(s)\, j_{s=0\ :3} = 2000$$

and $f_0 = 1$. As one can see, Fig. 11, the augmenting function g(s) due to the strong decline with the saturation has a very short crossover region quickly reaching a constant value g(s) 1 at s 0:1, where the pendular regime begins. We note that we still use pressure-saturation relationship (6), which provides a reasonable approximation considering strong variations of permeability. Alternatively, the model can be easily generalized by using a Leverett J-function [32].

D. Numerical simulations and experimental results in three-dimensional spherically symmetric cases

To compare numerical solutions of the superfast di usion model (30) with experimental observations, we rst consider simulations in a three-dimensional spherically symmetric case, where saturations(r; t) is a function of time and the radius r in a spherical coordinate system with its origin at the centre of the hemisphere representing the wet volume, Fig. 4. We have started our simulations in this case with

$$s(r; t)\, j_{t=0} = s_f + s_a \cos^{\ a}(\ r = 2); \quad 0 \quad r \quad 1 \qquad (33)$$

at di erent values of parameters 0:2 s_a 1 s_f and 0:2 ${}_a$ 0:4. The value of L_0 then is de ned by conservation of the liquid, neglecting the evaporation e ects,

$$2 \int_0^{Z\ 1} s(r; 0)\, r^2\, dr = V_D\, L_0{}^3:$$

We note, that due to the use of a spherical coordinate system, we also require that atr = 0 the rst derivative @s=@r 0 to avoid singular spurious solutions.

The choice of parameters s_a in the initial distribution and even its functional form is not obvious. We observed in the experiments that just in about ten minutes of spreading, the wetting spot volume shape becomes spherically symmetric, when the average saturation level s 0:5, Fig. 5. But what is the liquid distribution at this stage?

If we x parameters of the initial distribution (s_a and ${}_a$) and parameter s_f, then evolution of the moving front at di erent values of s_f s_0^e represents a family of curves shown in Fig. 12. One may notice that, rst of all, the smaller is the parameters$_f$ s_0^e (that is the higher is the reduced capillary pressure at the moving front) the faster the spreading occurs. Secondly, the power law found in the experimentsV / A + B $(t=t_0)^{0:75}$ is very well observed in the simulations, see insert in Fig. 12.

As one can see from the distribution of the liquid att > 0, Fig. 13 (a)-(b), the saturation pro le quickly relaxes to a universal distribution at xed values of s_f, s_f s_0^e and V_D. The distribution s(r; t) at t = t_2 = 6 10 ^{5}, when the average value of saturation is alreadys 0:

FIG. 12. Simulation of spreading in a three-dimensional spherically symmetric case using augmented superfast di usion model (30) with initial distribution (33) at ${}_a$ = 0:3, s_a = 0:4, ${}_g$ = 16:5; ${}_g$ = 1:65; f_0 = 1 and s_f = 0:0052, but at di erent values of parameter s_f s_0^e. Normalised wet volume $V = V_D$ (inverse average saturation s ^{1}, solid lines) as a function of the reduced time $t=t_0$, $t_0 = L_0^2 = D_0^e$. From left to right: (I) s_f s_0^e = 0:0001, (II) s_f s_0^e = 0:0002, (III) s_f s_0^e = 0:0004, (IV) s_f s_0^e = 0:0008. Insert shows the power law $V = V_D = A + B\,(t=t_0)^{0:75}$ (solid line, brown) in comparison with the numerical data (symbols, black) at s_f s_0^e = 0:0008.

FIG. 13. Simulation of spreading in a three-dimensional

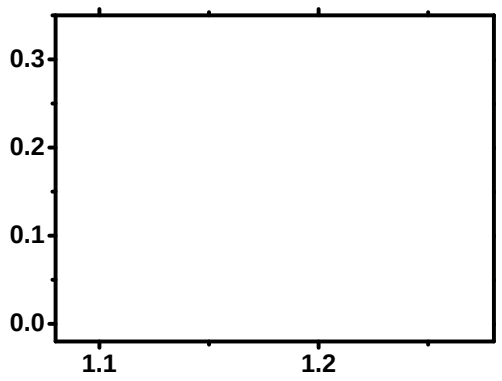

FIG. 14. Simulation of spreading in a three-dimensional spherically symmetric case using augmented superfast di u-sion model (30) with initial distributions given by (33) at $_a = 0:2$ and $s_a = 0:5$. Saturation $s(r;t)$ as a function of the reduced spot radius $r=L_0$ at xed values of $_g = 16:5$; $_g = 1:65$; $f_0 = 1$, $s_f = 0:0052$ and $s_f \quad s_0^e = 0:0002$. A compari-son between the asymptotic solution (34) (solid line, brown) and the numerical solution at $t = t_1 = 3 \quad 10^{6}$ shown by symbols, $W_0 \quad 287$. The insert shows a similar comparison, but at $t=t_0 = t_2 = 6 \quad 10^{5}$, $W_0 \quad 62$.

general case

$$X_n(t) / \quad t^{1=(n+1)} ;$$

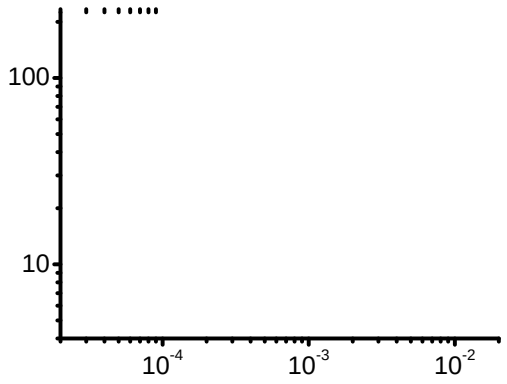
100
10
10^{-4}
10^{-3}
10^{-2}

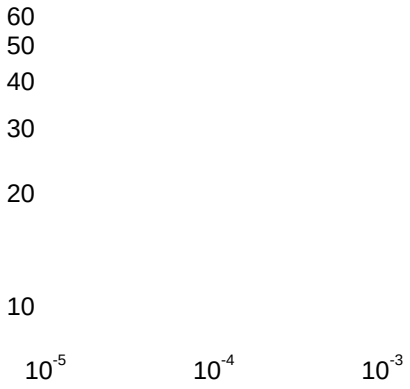

FIG. 17. Spreading TCP, TEHP and TBP liquid drops ($V_D = 3\,\mathrm{mm}^3$) in sands with $R = 0{:}25\,\mathrm{mm}$ in one-dimensional geometry. Comparison between experimental data and simulations using superfast di usion model model (30) with initial distribution of saturation given by (35). Normalised wet volume V/V_D (inverse average saturation s^{-1}) as a function of the reduced time t/t_0, $t_0 = L_0^2/D_f$. Experimental data are shown by symbols and simulation is presented by the solid line. Parameters of the simulations and the tting are summarized in Table I. The dashed line (brown) is the t $V/V_D = A + B(t/t_0)^{0:5}$ at A 8:5 and B 440.

expect that the distributions could be di erent due to the hysteresis e ect commonly observed in porous media spreading processes [32, 34, 35]. For example, if some areas on the grain surfaces were inaccessible to the liquid ow at low saturation levels [11], then during shaking and mixing those areas might be wet. The assumption is in agreement with the analysis presented in [11] and our observations that the equilibrium value of $_R$ 0:2 after natural spreading is small. That is, during the natural spreading, large surface areas of the grains were left dry. This implies that the liquid content in equilibrium would depend on the way this equilibrium was achieved, and this seemed to be observed in our experiments, Figs.

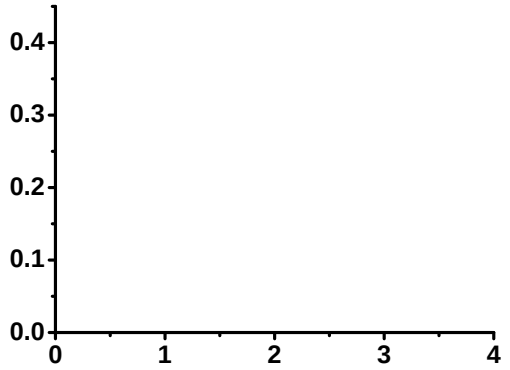

FIG. 20. Simulation of spreading of TEHP liquid drops (V_D = 6 mm^3) in pre-wetted sands with the background saturations level s_r = 1% using the augmented model (30) with initial conditions (36) at $s_a = 0:4$, $r_a = 4$ and $_a = 0:3$ with s_0^e 0:0068.

Hence, one can easily follow the evolution of a benchmark point $x_m(t)$, as is shown in Fig. 20. The result at s_r = 1%, shown in Fig. 19 in terms of the evolution of the volume contained within 0 r x_m, indicates that while there is some initial plateau in the distribution of the saturation, as is observed in the experiments presented in the same gure, in general the evolution is much slower. One can conclude then that, while the initial plateau observed during the volume evolution at high average saturation valuess 20% at both s_r = 2% and s_r = 1% indicates that the mechanism of spreading is sensitive to the background levels, see Fig. 19, to the large extent the spreading dynamics is still de ned by the front capillary pressure generated on the scale of surface roughness. One can also conclude that the liquid morphology of that background liquid distribution seemed to be di erent from the liquid morphology observed at these saturation levels during the natural spreading.

In the second case $s_r < s_0^e$, one needs to modify the original model to include the presence of some background saturation level. Using conservation of the liquid in the domain with a front @(t) moving into the area with background saturation s_r and the transport Reynolds theorem

$$\frac{d}{dt}\int_{(t)} s\,d^3x = \int_{(t)} \frac{@s}{@t} + r \quad (sv) \quad d^3x =$$

$$= \int_{@(t)} (v \quad n)\, s_r\, dS;$$

where n is the normal vector to @.

Transforming the surface integral into the volume integral

$$\int_{(t)} \frac{@s}{@t} + r \quad ((s \quad s_r)v) \quad d^3x = 0:$$

This implies that an equivalent moving boundary-value non-linear di usion problem of transport in pre-wetted sands can be formulated in terms of a function = s s_r

$$\frac{@'}{@t} = r \quad \frac{c_0(' \quad)\, g(' \quad)r\, '}{j\ln(' \quad ' \quad _0)j(' \quad ' \quad _0)^{3=2}}; \qquad (37)$$

$$' \quad _0 = s_0^e \quad s_r$$

with the boundary conditions

$$' \; j_{@} = s_f \quad s_r$$

and

$$v_n j_{@} = \frac{c_0(' \quad)\, g(n \quad r\,)'}{(s_f \quad s_r)j\ln(s_f \quad s_0^e)j(s_f \quad s_0^e)^{3=2}}: \qquad (38)$$

One can see that in general due to a smaller factor at the moving front s_f s_r (instead of just s_f), the front motion is expected to proceed with much higher velocity. This is understandable, since one require(is)-336ts understandable

CONCLUSIONS

In our previous study we established that:

The process of spreading can be described by a special type of non-linear di usion process, where the driving force is the capillary pressure at the moving front generated by the particle surface roughness and the coe cient of di usion has a characteristic singular form $D(s) / (s \quad s_0^e)^{\ 3=2}$. The resulting mathematical model belongs to a class known as super-fast di usion equation, and the so-suggested scaling with viscosity and surface tension is as expected for capillary ows, $D / \quad = \ .$

Motion of the wetting front $X_3(t)$ in a three-dimensional spherically symmetric domain (when the wetted volume has a shape of the hemisphere) exhibits universal scaling behaviour with time t, such that $X_3(t) / \ t^{1=4}$, ultimately going to stand-still at nite saturation levels $s_0 \quad 0{:}6\%$. This behaviour led us to a conjecture, con rmed in numerical simulations of the superfast di usion model, that in general, depending on the geometry, basically on its dimension n, $X_n(t) / \ t^{1=(n+1)}$, which may be used in practical applications to analyse such kind of spreading processes.

the surface of grains was solely de ned by the surface roughness, at least for the well-wetting liquid-solid combinations used in our study. Such universal behaviour allows to predict one of the main parameters of the models$_f$ s_0 with su cient accuracy only on the basis of the e ective surface area S_T / 1=R, porosity and the average amplitude of the surface roughness$_R$.

One can then nally conclude that on the basis of comparison with experimental data the augmented superfast non-linear di usion model (30) provides adequate description of liquid transport at low saturation levels, which therefore can be used in practical applications.

[1] Herminghaus, S., Dynamics of wet granular matter Adv. Phys. 54, 221, (2005)

[2] Scheel, M.; Seemann, R.; Brinkmann, M.; Michiel, M.D.I.; Sheppard, A.; Breidenbach, B. and Herminghaus, S., Morphological clues to wet granular pile stability Nature Mater. 7, 189, (2008)

[3] Scheel, M.; Seemann, R.; Brinkmann, M.; Michiel, M.D.I.; Sheppard, A. and Herminghaus, S., Liquid distribution and cohesion in wet granular assemblies beyond the capillary bridge regime J. Phys. Condens. Matter 20, 494236, (2008)

[4] Melnikov, K.; Wittel, F.K. and Herrmann, H.J., Micromechanical failure analysis of wet granular matter Acta Geotech. 11, 539{548, (2016)

[5] Orr, F.M.; Scriven, L.E. and Rivas, A.P., Pendular rings between solids: meniscus properties and capillary force J. Fluid Mech. 67, 723-742, (1975)

[6] Willett, C.D.; Adams, M.J.; Johnson, S.A. and Seville, J.P.K., Capillary Bridges between Two Spherical Bodies Langmuir 16, 9396{9405, (2000)

[7] Lukyanov, A.V.; Sushchikh, M.M.; Baines, M.J. and Theofanous, T.G., Superfast Nonlinear Di usion: Capillary Transport in Particulate Porous Media Phys. Rev. Lett. 109, 214501, (2012)

[8] Halsey, T.C. and Levine, A.J., How Sandcastles Fall Phys. Rev. Lett. 80, 3141-3144, (1998)

[9] Alshibli, K.A. and Alsaleh, M.I., Characterizing Surface Roughness and Shape of Sands Using Digital Microscopy J. Comput. Civil Eng. 18, 36-45, (2004)

[10] Tokunaga, T.K. and Wan, J., Water lm ow along fracture surfaces of porous rock Water Resour. Res. 33, 1287{1295, (1997)

[11] Or, D. and Tuller, M., Flow in unsaturated fractured porous media: Hydraulic conductivity of rough surfaces Water Resour. Res. 36

[36] Kulasiri, D. and Wynand Verwoerd, W., Stochastic Dynamics. Modeling Solute Transport in Porous Media. Series in Applied Mathematics and Mechanics 44, (North-Holland, 2002)

[37] Lee, T.E.; Baines, M.J. and Langdon, S., A Finite Difference Moving Mesh Method based on Conservation for Moving Boundary Problems J. Comput. Appl. Math. 288, 1{17, (2015)

[38] Baines, M.J., A Positivity- and Monotonicity-preserving Moving-mesh Finite Di erence Scheme based on Local Conservation Mathematics Report 1/17, (2017) Department of Mathematics and Statistics, University of Reading, UK, http://www.reading.ac.uk/web/ les/maths/semi-implicit.pdf

APPENDIX: NUMERICAL MOVING MESH METHOD.

The numerical technique used to solve the partial differential equations in this study is a moving mesh method driven by conservation, similar to that presented in [37] and described in [38]. A nodal velocity v is constructed from a combination of a non-linear di usion equation, for example the 3-D radially symmetric nonlinear di usion equation

$$\frac{@s}{@t} = \frac{1}{r^2}\frac{@}{@r}\left[r^2 D(s)\frac{@s}{@r}\right];$$

and the conservation law

$$\frac{@s}{@t} + \frac{1}{r^2}\frac{@}{@r}\left[r^2 sv\right] = 0; \tag{39}$$

yielding the velocity formula

$$v(r;t) = -\frac{D(s)}{s}\frac{@s}{@r} \tag{40}$$

where $v(0;t) = 0$. An equation for $ds=dt$ following the motion is then

$$\frac{ds}{dt} = \frac{@s}{@t} + v(r;t)\frac{@s}{@r} = -\frac{1}{r^2}\frac{@}{@r}\left[r^2 sv\right] + v(r;t)\frac{@s}{@r}$$

$$= -s\frac{1}{r^2}\frac{@}{@r}\left[r^2 v\right] = -s\frac{1}{r^2}\frac{@}{@r}\left[r^2\frac{D(s)}{s}\frac{@s}{@r}\right] \tag{41}$$

Introducing moving nodes $b_i(t)$ and corresponding saturation values $s_i(t)$; $(i = 1;\ldots;N)$, an approximation to (40) is

$$v^n_{i+1=2} = -\frac{D(s^n_{i+1=2})}{s^n_{i+1=2}}\frac{s^n_{i+1} - s^n_i}{b^n_{i+1} - b^n_i} \tag{42}$$

The system (41) is approximated by the first-order-in-time semi-implicit scheme

$$\left(\frac{s^{n+1}_i - s^n_i}{t} = \frac{s^n_i}{(b^n_{i+1=2} - b^n_{i-1=2})(b^n_i)^2}\right.$$
$$\left.(b^n_{i+1=2})^2\frac{D(s^n)}{s^n}_{i+1=2}\frac{(s^{n+1}_{i+1} - s^{n+1}_i)}{(b^n_{i+1} - b^n_i)} - (b^n_{i-1=2})^2\frac{D(s^n)}{s^n}_{i-1=2}\frac{(s^{n+1}_i - s^{n+1}_{i-1})}{(b^n_i - b^n_{i-1})}\right) \tag{43}$$

$(i = 1;\ldots;N-1)$ where t is the time step, which has the property that no new local extrema in s_i are created in the interior of the domain in a time step, thereby preserving positivity of s_i and avoiding oscillations. This allows arbitrarily large numbers of nodes without t being restricted by stability conditions.

The scheme (43) can be written in the matrix form

$$B\underline{s}^{n+1} = \underline{s}^n \tag{44}$$

where $\underline{s}^{n+1} = \{s^{n+1}_i\}$, $\underline{s}^n = \{s^n_i\}$, and B is a tridiagonal matrix modi ed to take into account the boundary condition $s_N = s_f$ and the continuity condition $@s=@r = 0$ at $r = 0$.

Once the s^{n+1}_i have been obtained the mesh nodes b^{n+1}_i can be found from the Lagrangian form of the conservation principle (39), i.e.

$$\int s(r;t)r^2 dr \text{ is constant in time,} \tag{45}$$

valid when $s(r;t) > 0$.

A discretisation of (45) is

$$\left\{(b^{n+1}_{i+1})^3 s^{n+1}_{i+1} - (b^{n+1}_i)^3 s^{n+1}_i\right\} = \text{its initial value} \tag{46}$$

$(i = 2;\ldots;N)$, yielding b^{n+1}_i by recursion over i, given $b^{n+1}_0 = 0$. Since the s^{n+1}_i are